Biocatalysis and Agricultural Biotechnology 21 (2019) 101327

Contents lists available at ScienceDirect

Biocatalysis and Agricultural Biotechnology

journal homepage: http://www.elsevier.com/locate/bab

Green biogenic synthesis of zinc oxide nanoparticles using *Pseudomonas putida* culture and its *In vitro* antibacterial and anti-biofilm activity

Jayaprakash Jayabalan [a,*], Ganesh Mani [b], Nandhini Krishnan [a], Johnthomas Pernabas [a], John Milton Devadoss [a], Hyun Tae Jang [b,**]

[a] Department of Microbiology, St. Joseph's College of Arts and Science (Autonomous), Cuddalore, Tamil Nadu, India
[b] Department of Chemical Engineering, Hanseo University, 360 Daegok-ri, Seosan-si, 356 706, Chungcheongnam-do, South Korea

ARTICLE INFO

Keywords:
Microbial synthesis
Zinc oxide nanoparticles
Pseudomonas putida
antibacterial activity
Antibiofilm activity

ABSTRACT

In the present work we demonstrated an environmentally acceptable biogenic synthesis of ZnO NPs using *Pseudomonas putida* (MCC 2989) broth culture. The physiochemical and morphological characters of the synthesized ZnO NPs was confirmed using UV–vis spectroscopy, XRD, SEM-EDX, and FTIR. The anti biofilm and anti bacterial activity of the synthesized ZnO NPs were studied against *Pseudomonas otitidis* (MCC 2509), *Pseudomonas oleovorans* (MCC 2566), *Acinetobacter baumannii* (MCC 2366), *Bacillus cereus* (MCC, 2039), and *Enterococcus faecalis* (MCC, 2041) using MTP and disk diffusion assay. The UV–Vis spectra show maximum absorbance of 300 and 310 nm for supernatant and isolated ZnO pellet, respectively, with a corresponding band gap of 4.00 eV. The FTIR results show the evidence for the presence of C═O, CH, and NH_2 groups, which proves the presence of remains of carbohydrates and amino acids from the bacterial culture used that is responsible for the formation of nanoparticle as well as for its stabilization. The results of anti-biofilm activity by MEP assay proved that the green synthesized ZnO NPs showed very potent activity against the tested microbial biofilms. Further, the ZnO NPs possess great anti microbial activity against the tested gram (+) and gram (−) ve microbes.

1. Introduction

Nanotechnology is an promising branch engineering science that involves in synthesizing and manipulating particles with specified shape and size below 100. Various nanoparticles like Fe, Ni, Co, Mn, Zn, etc. are widely-known and accepted nano materials for a variety of applications such as in catalysis, bio imaging, anti oxidants, and in life science as antimicrobials (Sharma et al., 2010; Ingale and Chaudhari, 2013; Anandalakshmi et al., 2016; Thaya et al., 2016; Fawcett et al., 2017; Ganesh et al., 2019). Further, nanoparticles are used in medical sciences in cases of drug delivery, imaging, and diagnostic tool. Nanoparticles possess a high surface area to volume ratio due to their small size, which leads to the very distinctive features of nanoparticles (Korbekandi and Iravani, 2012).

Nanoscience fields are growing rapidly on various fronts due to their completely new or enhanced properties based on size, distribution, and morphology (Khalil et al., 2013). Nanoparticles are swiftly attracting attention in areas such as health care, cosmetics, biomedical, food and feed, drug delivery, environment, and health applications (Kaviya, and Viswanathan, 2011). The synthesis of metal and metal oxide nanoparticles using a green approach is considered to be an environmentally friendly, cost effective, biocompatible, safe and valuable approach (Abdul et al., 2014). The phytochemicals from the plant extract and secondary metabolites from micro organisms may act as both reductant and capping or stabilizing agents for NP production (Auld, 2001; Xiao et al., 2016; Alijani et al., 2019; Shervani and Yamamoto, 2011).

The clean, non-toxic, and environmentally acceptable metal nanoparticles are hydrophilic in nature, dispersed uniformly in aqueous media, highly stable, and have shown enormous antimicrobial activity (Jayaseelan et al., 2012; Chan and Matdon, 2013). ZnO is one among the non-toxic metal oxide nanoparticles that acts as a strong antibacterial agent, and it has bactericidal activity on both gram positive and gram negative bacteria. Using ecologically beneficial materials like plant extracts, bacterial cellular extract, fungi, and enzymes for the synthesis of ZnO NPs leads to abundant benefits in terms of eco-friendliness and compatibility for a wide range of pharmaceuticals (Shankar et al., 2004).

* Corresponding author.
** Corresponding author.
E-mail addresses: prakash.j68@gmail.com (J. Jayabalan), htjang@hanseo.ac.kr (H.T. Jang).

https://doi.org/10.1016/j.bcab.2019.101327
Received 24 April 2019; Received in revised form 30 August 2019; Accepted 31 August 2019
Available online 31 August 2019

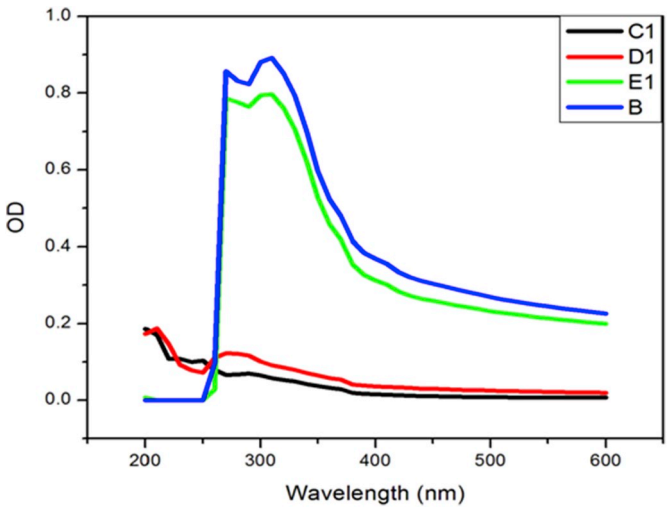

Fig. 1. UV–Vis spectrum of *Pseudomonas putida* growth kinetics at different time intervals (C1) - control (broth medium), (D1)- 6 h culture, (E1)- 24 culture, (B1)- 48 culture.

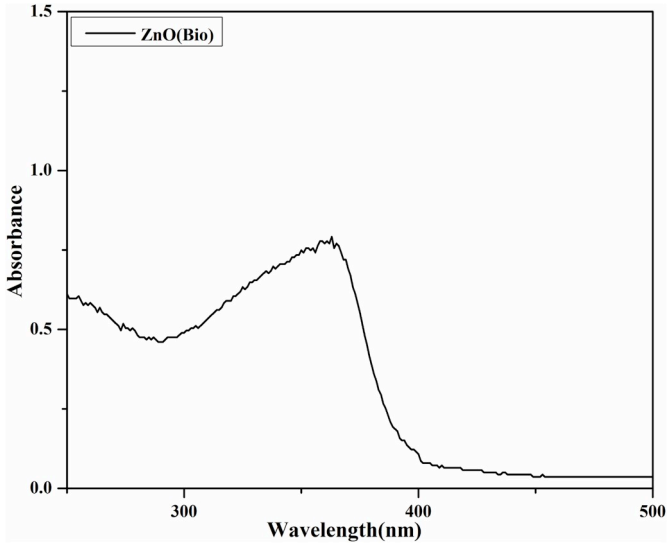

Fig. 2. UV–Vis spectrum of synthesized ZnO nanoparticles (a) Zinc oxide NPs extracted from reaction mixture (b) UV-DRS spectrum of Calcinned ZnO NPs.

Many organisms of both unicellular and multi cellular structure mediate formation of nano sized materials, either by intracellular or extracellular route. Recent studies on metal oxide nanoparticles evidences the antimicrobial activity including cell death in eukaryotic as well as prokaryotic cells (Nel et al., 2006; Long et al., 2006; Magrez et al., 2006) and show growth inhibition in due to cytotoxicity of the nano particle.

Pseudomonas putida (MCC 2989) a gram-negative, rod-shaped, soil bacterium that has the ability to degrade hydrocarbon (Marques and Ramos, 1993) and can utilize a wide variety of organic compounds as energy sources. It has been shown to be relatively efficient in the bioaccumulation of heavy metals from polluted effluents *P.putida* CZ1 possesses the tolerance to growt in the presence of metals (Cu, Zn) as well as it has high metal uptake capacity in aerobic conditions. Therefore, it can be potentially applicable for the in situ bioremediation of heavy metal-contaminated soil and water. The microbial process for the production of nanoparticles can take place either intracellularly or extracellularly (Ahmad et al., 2007; Jain et al., 2011). Extracellular biosynthesis is cheap and requires simpler downstream processing.

Hence, in this research ZnONPs were prepared by microbial synthesis using *Pseudomonas putida* (MCC 2989) broth culture. The biologically developed product was characterized for its physiochemical and morphological characters with the aid of UV–visible, UV-DRS, FTIR, XRD, and FE- SEM- EDX and TEM. In addition, we have also evaluated the *in vitro* biological characterization such as Growth analysis, congo red agar test, anti-biofilm activity, and antibacterial activity of synthesized ZnO NPs.

2. Materials and methods

2.1. Bacterial strains and chemicals

Pseudomonas putida (MCC 2989), *Pseudomonas otitidis* (MCC 2509), *Pseudomonas oleovorans* (MCC 2566), *Acinetobacter baumannii* (MCC 2366), *Bacillus cereus* (MCC 2039), and *Enterococcus faecalis* (MCC 2041) were obtained from Microbial Culture Collection (MCC), Pune, India. The culture samples were lyophilized and resuspended in tryptic soy broth (TSB) at 37 °C for 24 h so as to retain their natural or viable nature. The strains were grown under aerobic conditions at 37 °C in glass culture tubes with shaking at 150 rpm with light source-equipped shaker incubator. All the chemicals such as Zinc nitrate, Nutrient agar, Muller Hinton agar, Tryptic Soy Broth, and Muller Hinton broth were purchased from HiMedia Laboratories Pvt. Ltd., Mumbai, India.

2.2. Preparation of broth culture

The *Pseudomonas putida* strain was successfully revived in both Tryptic Soy Broth (TSB) and Tryptic Soy Agar (TSA) at 37 °C. A single colony was then inoculated in TSB (25 mL) in 250 mL conical flasks, which was then cultured at 37 °C and 150 rpm 24 h cultures were aliquoted with a dilution of 1:100 in TSB medium. Microbial growth measurements were taken at 600 nm using a spectrophotometer (UV–Vis (Spectramax^R Plus 384, St.Josephs college, Cuddalore). *Pseudomonas putida* (MCC 2989) was inoculated into TSB broth media under the aseptic condition of laminar flow. It was then placed in a shaker incubator at 35 °C and 150 rpm for 24 h.

2.3. Growth viability

Growth kinetics were essentially investigated by a UV–visible spectrophotometer with different intervals (6, 24, 48 h and control) of incubated *P.putida* broth culture at 600 nm. The control broth (without Zinc nitrate) value as compared with zinc nitrate added culture broth optical density value was plotted. After 48 h, the microbial viability in the presence or absence of with and without zinc nitrate culture broth were determined by UV–visible at O.D 600.

2.4. Growth analysis of Pseudomonas putida

A 50 mL overnight *P. putida* (MCC 2989) culture was grown in a 100 mL flask in Tryptic soy broth (TSB). Then, 10 mL of overnight culture was transferred into 100 mL of fresh culture medium (TSB), which was then incubated at 37 °C in a shaking incubator. Cultured samples were taken at different time intervals, a 5 mL aliquot was sampled from *P. putida* culture, and then the sample was transferred to a 10 mm corvette, and the optical density was measured at 600 nm (Mytilinaios et al., 2014).

2.5. Synthesis of ZnO nanoparticles by P.putida

Pseudomonas putida (MCC 2989) cells were allowed to grow as a broth culture in sterile distilled water containing tryptic soy broth media for 24 h. First, 25 mL of culture was taken and diluted with 75 mL of sterile distilled water containing nutrients. This diluted culture solution was then allowed to grow again for another 24 h. Next, 100 mg Zn $(NO_3)_2$ were added to the culture solution, and it was kept at 37 °C with

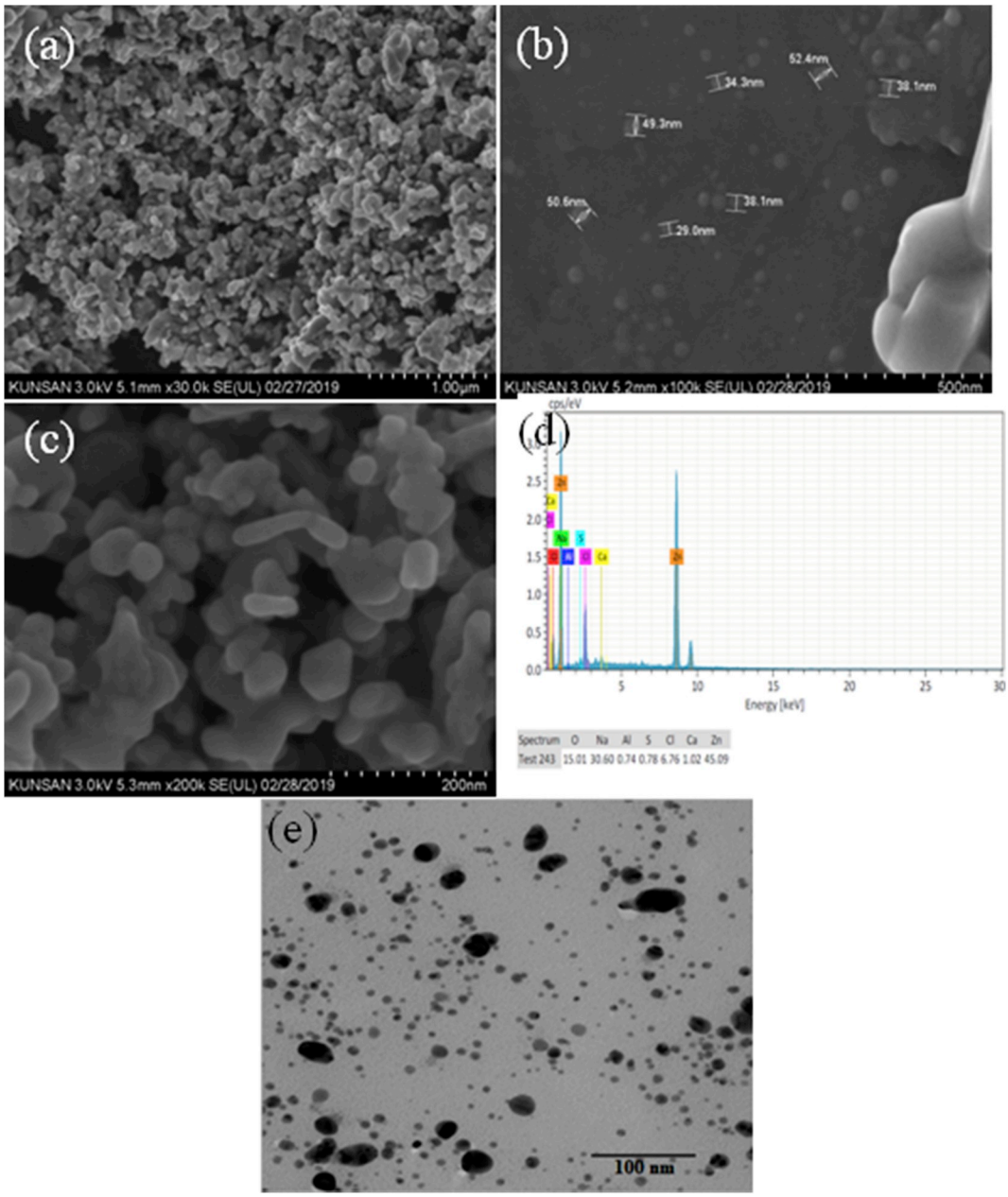

Fig. 3. FE-SEM and TEM microscopical images of synthesized zinc nanoparticles (a) particles at 1 μm scale (b) results of particle size measurement (with scale bars) (c) particles at 200 nm scale (d) FE-SEM-EDX spectrum of synthesized zinc nanoparticles (e) TEM image of synthesized zinc nanoparticles.

150 rpm for 24 h until white deposition began to appear at the bottom of the conical flask, indicating ion transformation. The culture solution was cooled and allowed to incubate at room temperature. After 12–48 h of rotary shaker incubation, the reaction mixture showed distinctly visible coalescent white clusters deposited at the bottom of the flask. After incubation, broth culture was centrifuged at 5000 rpm for 15 min. Supernatant and pellet were separated and dried for further study. The supernatant was kept in the petridish, and it was allowed to dry for the preparation of solid powder sample in the hot air furnace 400 °C for 2 h (Kirthi et al., 2011; Prasad et al., 2011).

2.6. Characterization of zinc oxide nanoparticles

The optical property of Zn NPs was determined by a UV–Vis spectrophotometer (spectra max ^{R} plus 384) in the 200–800 nm range operated at a resolution of 1 nm. And the diffuse reflectance UV (DRS Uv) spectra of the solid calcinned sample was recorded using Sinco Neosys 2000 UV (Korea) in DRS mode. The powder X-ray diffraction (PXRD) pattern of the synthesized particle ZnO NPs was screened using the Rigaku Miniflex diffractometer (TX, USA) by scanning between 10° and 70° (2θ) with Cu Kα radiation ($\lambda = 1.54$ Å) in steps of 0.02° step. FTIR spectra of the samples were recorded using a Bruker spectrum FTIR spectrophotometer in the scanning range of 4000–400 cm^{-1} wave number with up to 40 cycle. The shape, morphology, and elemental composition of the synthesized ZnO NPs were assessed using Field Emission Scanning electron microscopy (FE-SEM, FEI Quanta200) coupled with energy dispersive spectroscopy (EDX). To confirm the morphological features and size particle size of the ZnO NP's were observed using a Hitachi tunnelling electron microscope (Hitachi-800 TEM). The NP dispersion was placed over a copper grid and analyzed. The diameters of the nanoparticle were measured using the external image visualization software, Image-J (National Institutes of Health, USA). An X-ray photoelectron spectrum for the synthesized nanoparticles was carried to determine the surface purity and oxidation state

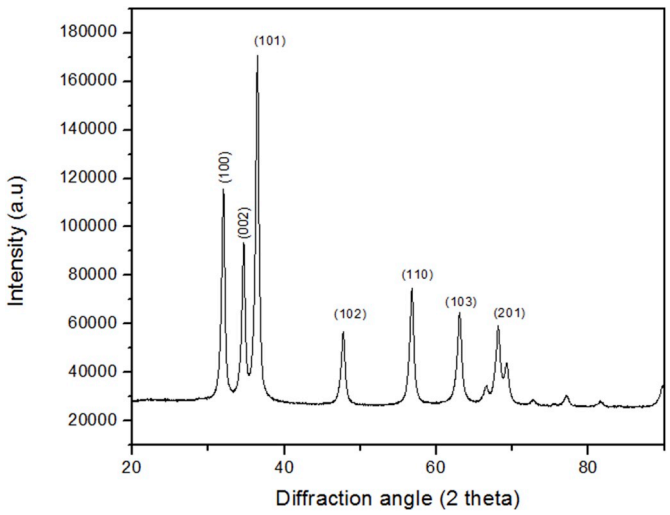

Fig. 4. XRD pattern of synthesized calcinned ZnO NPs.

of ZnO NPs synthesized using a PHI 5000 VersaProbe III (2017) photoelectron spectrometer equipped with Al Kα X-ray as source.

2.7. Congo red agar (CRA) test

The biofilm production of strains (MCC) was evaluated by the Congo red agar method (CRA), as reported by Freeman et al. (1989). All strains were cultivated on BHIA and 0.08% (w/v) congo red supplemented with 5% (w/v) glucose (Fitzpatrick et al., 2005). Following sterilization, the aqueous congo red was added when the agar was cooled to 55 °C. Plates were inoculated in a spot and incubated aerobically for 24 h at 35 °C, followed by storage at room temperature for 48 h. A positive result was indicated by black colonies with a dry crystalline consistency (Cotter et al., 2009). Six strains were inoculated per plate, and each experiment was performed at least three times.

2.8. Anti-biofilm activity

In order to evaluate the efficacy of ZnO NPs in interrupting bio-film formation, MTP assay, as portrayed by Christensen et al. (1985), was carried out. Individual wells of 96 well microplate were filled with 180 µL BHIB, followed by inoculation with 10 µL of overnight pathogenic bacteria cultures (Biofilm producer), such as *Bacillus cereus* (MCC 2039) and *Enterococcus faecalis* (MCC 2041), followed by 10 µL of ZnO NPs from the prepared stock solution of 10, 20, 30, 40, and 50 µg/mL, respectively, along with control, and incubated for 24 h at 37 °C. After the incubation contents were removed from the wells, they were washed with 0.2 mL of normal saline to remove free-floating bacteria. The adhered sessile bacteria was fixed with sodium acetate (2%) and stained with crystal violet (0.1% w/v). The excessive stain was removed by deionised water washing and dried. Finally, the dried plates were washed with 150 µL of 95% ethanol, and optical density was recorded using a UV–Vis spectrophotometer (Spectramax^R Plus 384) at 595 nm.

2.9. Antibacterial activity

The media used in this assay was Muller Hinton Agar and Tryptic soybean broth (TSB). The media was prepared according to the manufacturer's direction. A 24 h Muller Hinton Broth culture of tested bacteria was grown in a shaking incubator, washed twice with phosphate buffer solution, and then standardized to approximately 10^6 CFU/mL using broth medium. The antibacterial capability of synthesized ZnO NPs on the selected pathogens of clinical importance was determined by the agar well diffusion assay (Wahab et al., 2010). For the antibacterial activities wells made in the plate were filled with Muller Hinton Agar (MHA) seeded with 24 h of each clinical isolate of various MCC Strains. The concentrations ranging from 30, 60, 90, and 120 µg/µL of ZnO NPs were placed in respective well, along with the control. The plates were then incubated at 37 °C for 24 h. The diameters of the inhibition zones were measured and tabulated.

3. Results and discussions

3.1. UV–vis spectroscopy

Fig. 1 depicts the trends in bacterial growth analysis in relation to optical density (O.D) at particular time intervals. The graph indicates better growth and viability of *P.putida* in culture broth. Fig. 2 shows the UV–Visible spectra of the ZnO nanoparticles developed by the bacterium (*P.putida*). The surface Plasmon resonance (SPR) was observed at 360 nm for calcinned sample by UV -DRS that proves the formation of

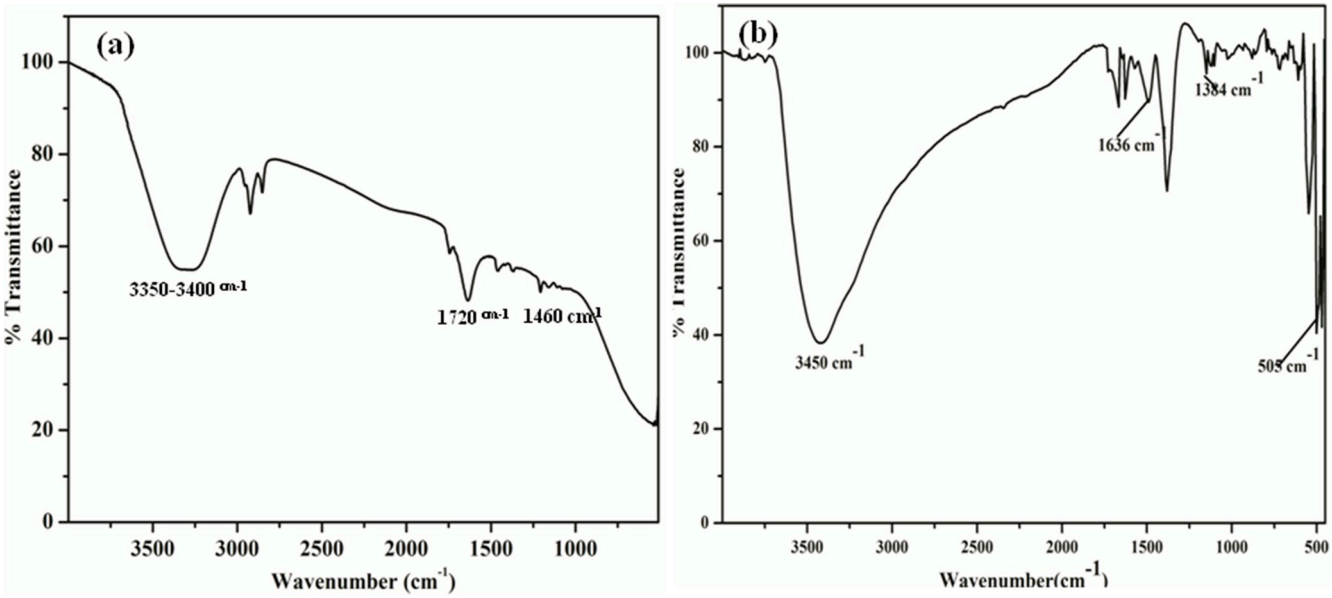

Fig. 5. FTIR spectra of (a) culture media and (b) biogenic ZnO NPs after calcinations.

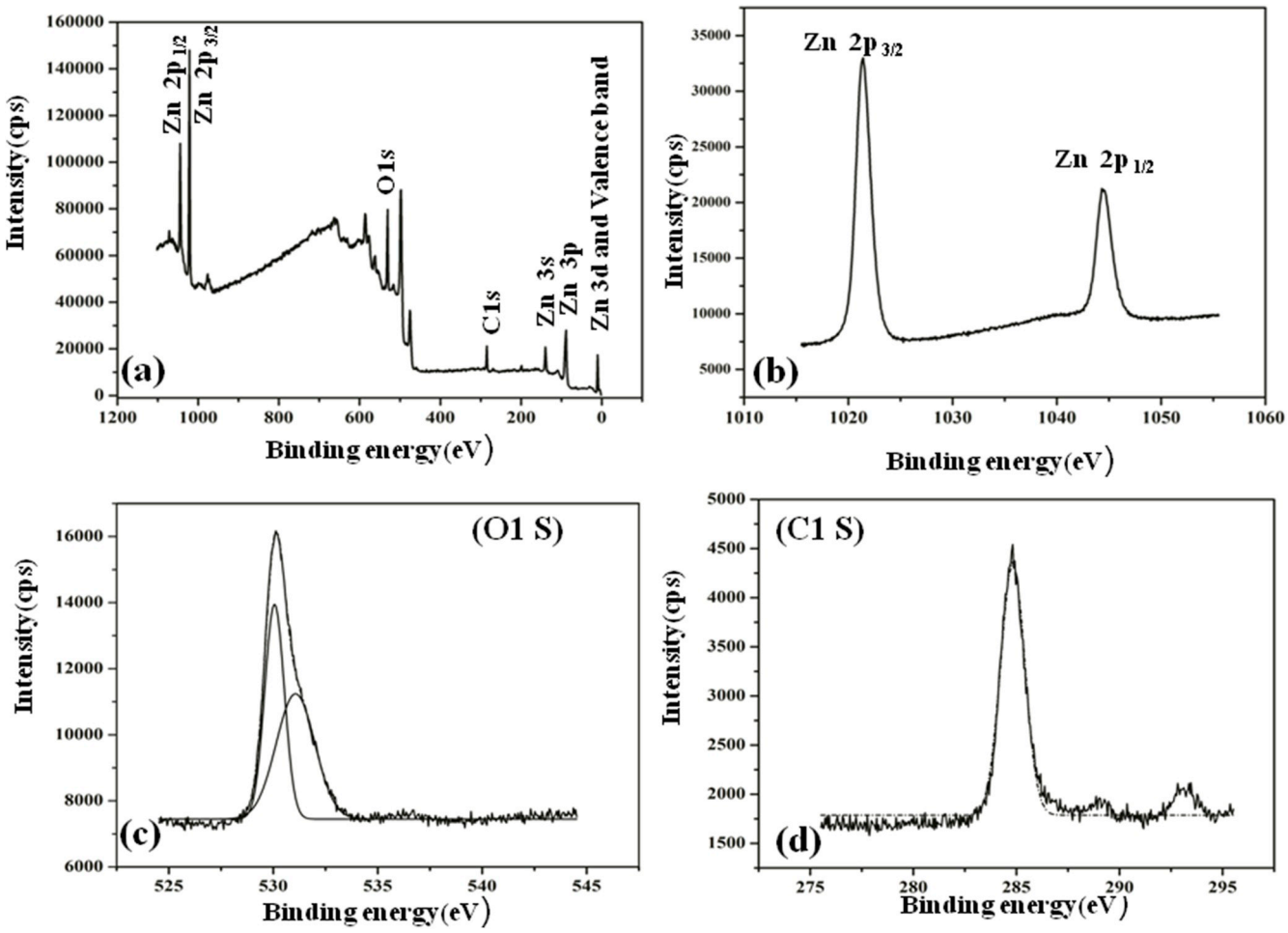

Fig. 6. XPS spectrum of ZnO NPs (a) full scan survey (b) deconvoluted single component BE peaks of Zn (c) O1s BE peak (d) C1s BE peak.

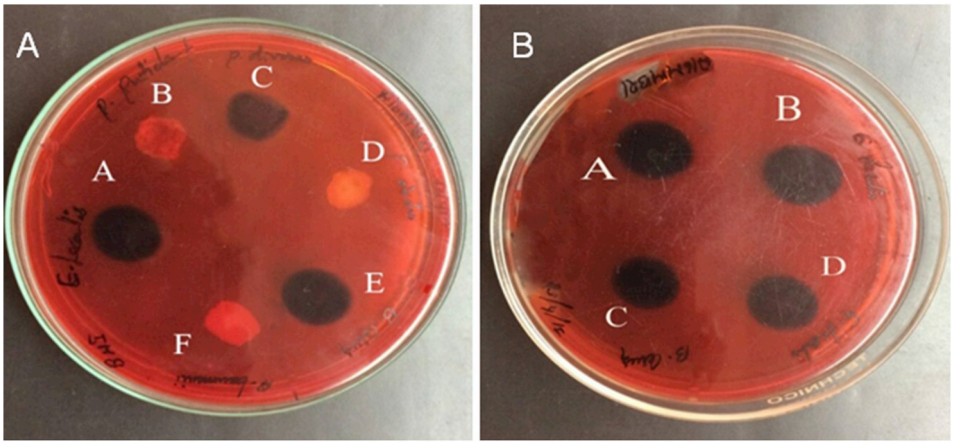

Fig. 7. Bio-film production on Congo red method A) red colonies, non bio-film producer: B) bio-film producer appeared black color.

ZnO Nps. The corresponding band gap was calculated using the formula $E_g = 1240/\lambda$ and it was found to be 4.00eV. This serves as evidence for the successful formation of ZnO NPs. These results are in good agreement with the earlier report on the synthesis of ZnO NPs using microorganisms (Jayaseelan et al., 2012). The mechanism behind the extracellular synthesis of nanoparticles using microbes is yet to be fully understood. However, it is capable of producing some enzymes, like nitrate reductase secreted by microbes help in the bio reduction of metal ions to metal nanoparticle.

3.2. FE-SEM - EDX and TEM

Fig. 3(a–d) shows the FE-SEM images with EDX spectrum of ZnO nanoparticles. From the FE-SEM image, it could be observed clusters of spherical agglomerated observed in nano-sized with particle diameter in the range of 25–45 nm. The EDX micrograph presented in Fig. 3(b) showed the purity of the ZnO compound. Results of EDX showed for the presence of other elements such as O, Na, Al, S, Ca, and S. According to the EDX report, the weight percentage and atomicity of Zn and O were

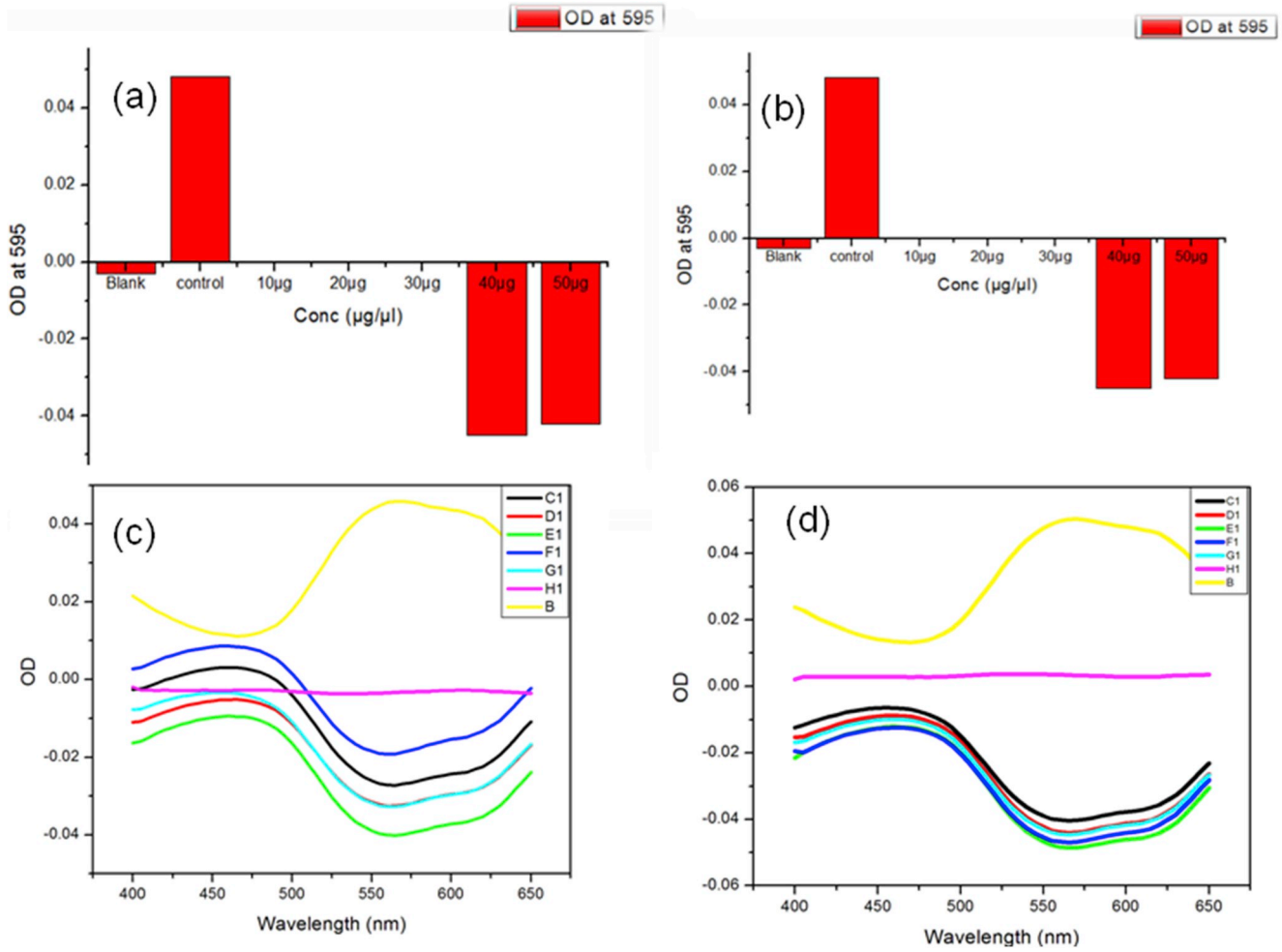

Fig. 8. In-vitro anti bio-film activity of ZnO NPs against (a) *E. faecalis*,(b) *B. cereus,* and Dose depended UV–Vis spectrum for bio film inhibition by ZnO NPs against (c) *E.faecalis* (d) *B.cereus* (H1) blank solution (B) Control (absence of ZnO NPs), (C1) 10 µg ZnO NPs, (D1) 20 µg ZnO NPs, (E1) 30 µg ZnO NPs(F1) 40 µg ZnO NPs, (G1) 50 µg of ZnO NPs.

found to be 45.09% and 15.1%, respectively which is higher in percentage when compared to other element, the peak for other major elements such as Na, Cl and Ca may arises from the broth media used and presence of Al is due aluminium stub of FE-SEM. Results of TEM analysis was presented in Fig. 3(d) which shows the particles were in spherical morphology with average diameter of 44.5 nm with reference to the analysis carried out using image-J. These results support the size and morphology obtained with FE-SEM.

3.3. XRD

Fig. 4 shows typical X-ray diffraction patterns of the developed ZnO NPs, with brags diffraction peaks were observed at $2\theta = 32.0$, 34.12,36.52,47.67,58.12,63,12 and 68.89 were indexed to (100), (002), (101), (102), (103) and (201) planes of ZnO exhibiting a crystalline wurtzite structure (JCPDS file: 89–1397) of ZnO with little shifting. These results confirm the phase purity of the obtained ZnO Nps. Further the average Dp (size)of the obtained ZnO Nps calculated using Scherrer's formula $Dp = 0.9\lambda/\beta \cos\theta$, where λ is the wavelength of X rays used (1.54 Å), β is the full width at half maximum (FWHM), and θ is the angle of diffraction obtained from the observed most intense peak of the sample. The found average size of the synthesized ZnO NP was found to be around 50 nm which similar with the particle size observed using FE-SEM and TEM.

3.4. FT-IR

Fig. 5(a) shows the FT-IR spectrum of the culture media before adding zinc nitrate. A broad peak observed at around 3400 cm^{-1} was attributed to the carbonyl and OH alcohol and phenolic carboxylic further a shoulder peak near 3400 cm^{-1} was due to –NH functionality of amino acids present in the culture media and a peak at 1720 cm^{-1} was attributed to C═O group of esters or carboxylic acid. The –CH bending vibrations of aldehyde or ketonic functionality were observed near 1460 cm^{-1}. Likewise the peak at around 1100- 1200 cm^{-1} was assigned to C–O–C vibration of and the other peaks that are expected to appear in the finger print regions were absent due to overcrowding of functional groups.

ZnO NPs (Fig. 5(b)), a broad peak observed from 3200 to 3500 cm^{-1} was attributed to the OH stretching vibration of the physically adsorbed water or phenolic OH amino acid such tyrosine or phenylalanine that remain after calcination that are arises from the extracellular protein from micro organism or from the media used. A peak at around 1024 cm^{-1} was due to carboxylic acid (-COO), while peaks at 1636 and 1384 cm^{-1} are assigned to the asymmetric and symmetric stretching of Zinc carboxylate that are remains after calcination OH peaks are due to the surface adsorbed water. Transmittance bands at 460 and 505 cm^{-1} are due to pure ZnO NPs further the peak at 460 cm^{-1} represents the hexagonal mode (E_2) of ZnO NP, which is little shifted from of 435 cm^{-1} of its original position because of the organic remains from the bacterial extracellular materials and form the nutrients in the culture media that

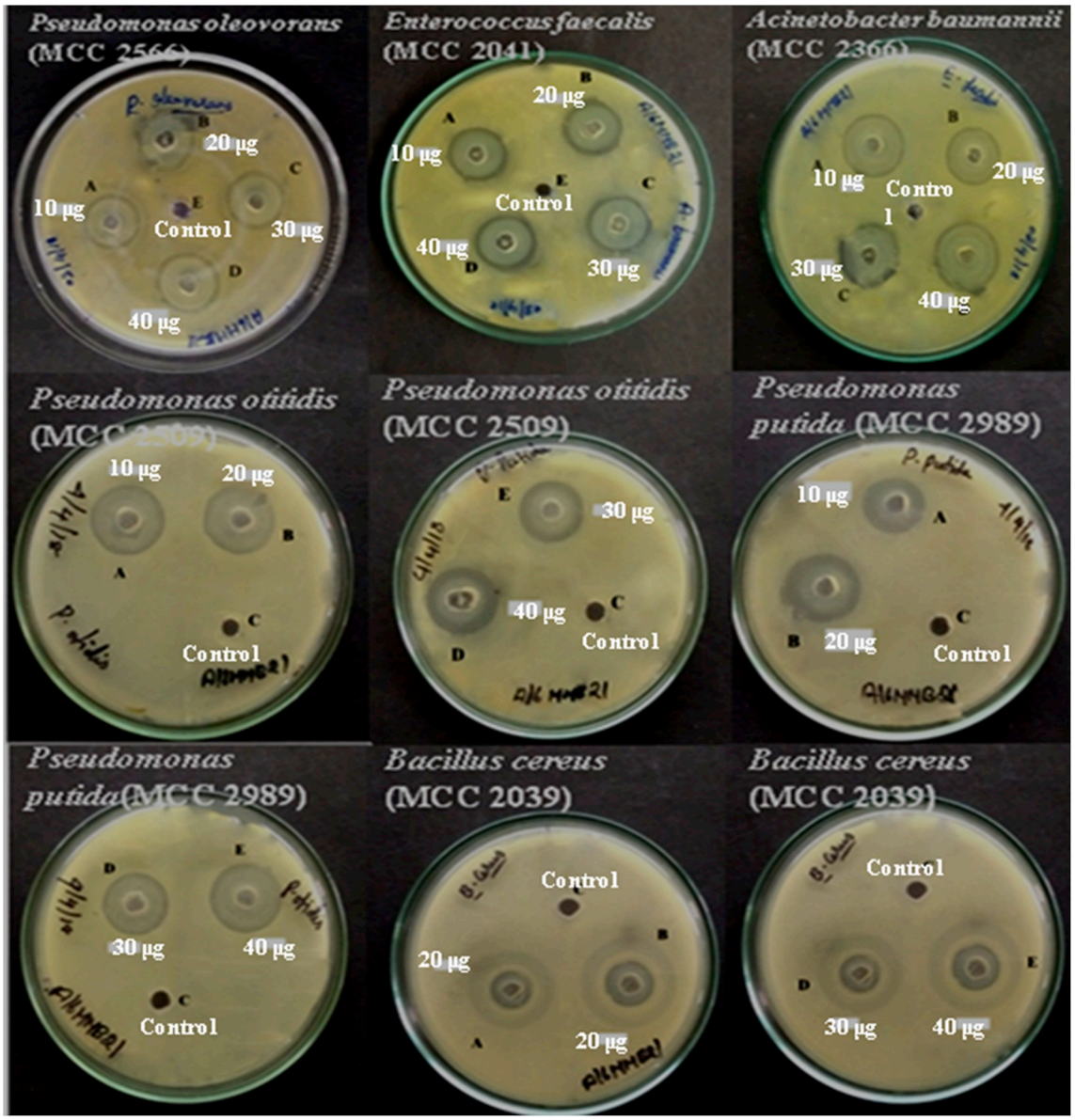

Fig. 9. Images for the antibacterial activity of *P.putida* synthesized ZnO nanoparticles against various clinical pathogens by agar well diffusion method.

are present over the ZnO NPs (Xiong et al., 2006).

3.5. XPS analysis

To confirm the surface purity and oxidation degree of the synthesized ZnO NP's XPS analysis was carried out. The outcome of the experiments depicted in Fig. 6. In that Fig. 6(a) portrayed the full survey scan of biogenic ZnO. In that, the peak for Zn 2p $_{1/2}$, Zn2p $_{3/2}$, O1S and C 1S were clearly appeared at the bonding energies of 1044.49(eV), 1021.52 (eV), 530(eV) and 284.83 (eV) respectively. The obtained the results suggest that the remains of partially oxidized organic molecule that were absorbed over the surface of ZnO NPs during the calcinations process. Fig. 6(b) shows the deconvoluted single component BE peaks of ZnO NPs, that shows the clear shifting of Zn $2p_{1/2}$ and Zn $2P_{3/2}$ BE of ZnO Nps from its original position with reference to the Auger parameter (AP) given in NIST XPS data base this may be due the absorbed carbonaceous matter with reference to the appearance of C1S BE (Fig. 6(d)) peak for the partial oxidized matters (Wagner et al., 2003). This was further supported by the appearance of O1S (Fig. 6(c))secondary shoulder BE peak for oxygen at BE 531.43 (eV) this evidences the presence of absorbed oxygen or partially oxidized carbonaceous matter C1S BE (Fig. 6(d)) at 284.83 (BE) that arises from the culture media or from the bacterial culture (Wagner et al., 2003; Rauwel et al., 2011; Steffy et al., 2018). The presence of such things along with the final ZnO NPs were further supported from the appearance of vibrational bands for (-COO) in FTIR spectra as discussed earlier.

3.6. Screening of biofilm producing strains by CRA test

The CRA test results indicate the biofilm producer (Fig. 7) among five clinical pathogens. All bacteria were inoculated onto CRA plates by the spot dot method, which produces a more uniform color, making them easier to identify the biofilm producer. The major colors were black or brown, indicating the biofilm producer, and red or dark red for the non – biofilm producers. Finally, *Enterococcus faecalis* and *Bacillus cereus* were identified as bio-film producers and selected for MTP assay (Barbara et al., 2009).

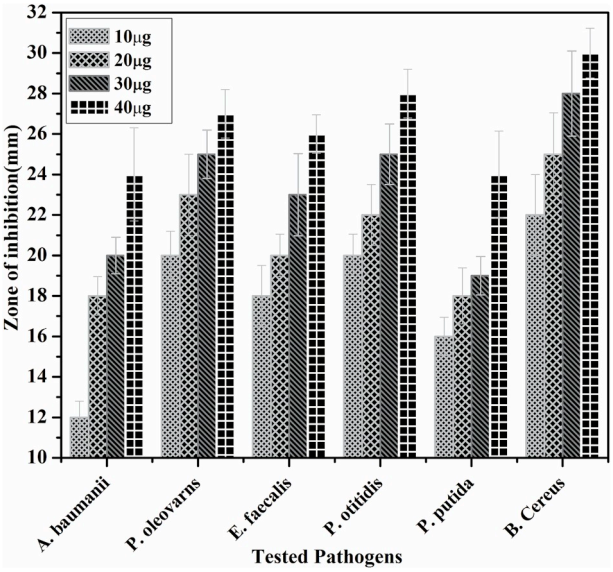

Fig. 10. Comparative Antibacterial activity of ZnO NPs at various concentrations against clinical pathogens.

3.7. Anti-biofilm activity (MTP assay)

ZnO-NPs possess an extreme level of action to destruct biofilm of selected pathogenic bacteria. The biofilm inhibition potency of microbial synthesized ZnO NPs against tested biofilm, producing bacteria such as *Enterococcus faecalis* shown in Fig. (8 a and c) and for *Bacillus cereus* (Fig. 8 b and d). The biofilm activity was high, even with the lowest quantity of ZnO NPs (10 µg/mL). Our results show ZnO NPs have a high degree of biofilm destruction against both gram-negative bacteria and gram-positive bacteria which is similar with that of previously demonstrated ZnO nanoparticles that inhibited the *P. aeruginosa* growth by ceasing the exo-polysaccharide synthesis and inhibiting biofilm formation (Christensen et al., 1985; Kalishwaralal et al., 2010; Ishwarya et al., 2018). This results proved that the synthesized ZnO-NPs nanoparticles can effectively and rapidly detach biofilm, which implies the application of nanoparticles as biofilm disrupting agents (Kalishwaralal et al., 2010; Ishwarya et al., 2018). The bio mechanism of anti biofilm activity exhibited by the biogenic synthesized ZnO NPs may due to the extracellular ROS production induced by the ZnO Nps that causes the destruction bio film exo-polysaccharides produced by microbes as explained previously (Ishwarya et al., 2018).

3.8. Antibacterial assay

The antibacterial stability and efficiency of the *P.putida* mediated ZnO NPs was tested against five clinical isolates such as *Bacillus cereus* (MCC 2039), *Pseudomonas otitidis* (MCC 2509), *Pseudomonas oleovorans* (MCC 2566), *Acinetobacter baumannii* (MCC 2366), and *Enterococcus faecalis* (MCC 2041). The bacterial inhibitory concentrations of ZnO NPs were 30, 60, 90, and 120 µg/µL, respectively. Fig. 9 and Fig. 10 show that microbial synthesized ZnO NPs significantly inhibited the growth of the clinical pathogens and the inhibition range of NPs treated with *Acinetobacter baumannii* (13–24 mm), *Pseudomonas otitidis* (14–23 mm), *Pseudomonas oleovorans* (10–18 mm), *Enterococcus faecalis* (14–26 mm), and *Bacillus cereus* (14–27 mm), respectively. Based on this above observed antimicrobial activity test, it is proven that the ZnO NPs have good and strong antimicrobial activity. In general Gram-positive bacteria have a multilayer of peptidoglycan polymer and a thicker cell wall (20–80 nm), and have teichoic acid and lipoteichoic acid in their structure that acts as a chelating agent and transport the zinc ion from ZnO NP into cell (Hood and Skaar, 2012; Kumar et al., 2011). Gram-negative bacteria cell wall is composed of a plasma membrane and thin layer of peptidoglycan layer (7–8 nm) and porins in the outer layer that facilitates passive diffusion of ZnO nanoparticles inside of the cell (Barapatre et al., 2016; Saravanakumar et al., 2015; Ganesh et al., 2019). Microbial developed ZnO nanoparticles were small enough in size that could efficiently pass through the peptidoglycan layer, and were highly susceptible to damage. When chelated Zn^{+} from zinc Oxide nanoparticles leads to loss of phospho-lipid bilayer integrity and release of intracellular components leads to cell death. Zn ion can interact with sulphhydryl group of enzymes and inhibit the enzymes like alkaline phosphatise, polymerases, carboxy peptidase. Zinc ions bind strongly with Cystein, Histidine, Aspartate side chains of proteins in nanomolar concentration (Chulhun and Herbert, 1995). During the bacterial cell wall destruction process, pathogenic organisms lose their osmotic pressure (ionic strength), and the cell functions, such as growth, metabolic activity, and replication, etc, were inhibited. ZnO NPs of smaller size can easily penetrate into bacterial membranes due to their large interfacial area, thus enhancing their antibacterial efficiency. NPs size was a crucial factor in achieving the best bactericidal and fungicidal response, and ZnO NPs with a smaller size showed the highest antibacterial activity (Barapatre et al., 2016; Saravanakumar et al., 2015; Ganesh et al., 2019; Zhang et al., 2007; Yamamoto, 2001; Sawai et al., 1996; Narendhran and Sivaraj, 2016).

4. Conclusions

In our study, the microbial synthesis of Zinc oxide nanoparticles using *Pseudomonas putida* (MCC 2989) has been reported. Nanoscience directs great attention toward the development of nanomaterials with more potent bioactivities. The method reported herein is a green and microbes-mediated low-cost approach that is capable of developing Zinc nitrate to Zinc oxide NPs at room temperature. This synthesized ZnO NPs was hexagonal in shape and crystalline in nature with an average size of 44.5 nm, as evidenced by XRD and FE-SEM with EDX analysis. As evidenced by FTIR, this indicates high activity of the nanoparticles to the relatively high levels of polysaccharide. From the results of antibiofilm assay, the synthesized zinc Oxide nanoparticles exhibited a high degree of biofilm detachment property in the different concentrations tested. The synthesized nanoparticles showed good antibacterial activity, which has inhibited the growth of Gram-negative and Gram-positive bacteria. In conclusion, this study found a possible means for developing zinc oxide nanoparticles conjugated antibiotics (adjuvant for antibiotics) that may enhance and boost up the activity of commercially available antibiotics in the future.

Conflicts of interest

The authors have no conflicting interest to declare.

Appendix A. Supplementary data

Supplementary data to this article can be found online at https://doi.org/10.1016/j.bcab.2019.101327.

References

Abdul, H., Sivaraj, R., Venckatesh, R., 2014. Green synthesis and characterization of zinc oxide nanoparticles from *Ocimum basilicum* L. var. Purpurascens Benth- *lamiaceae* leaf extract. Mater. Lett. 131, 16–18.
Ahmad, R., Minaeian, S., Shahverdi, H.R., Jamalifar, H., Nohi, A., 2007. Rapid synthesis of silver nanoparticles using culture supernatants of Enterobacteria: a novel biological approach. Process Biochem. 42, 919–923.
Alijani, H.Q., Pourseyedi, S., Torkzadeh Mahani, M., Khatami, M., 2019. Green synthesis of zinc sulfide (ZnS) nanoparticles using *Stevia rebaudiana Bertoni* and evaluation of its cytotoxic properties. J. Mol. Struct. 1175, 214–218.
Anandalakshmi, K., Venugobal, J., Ramasamy, V., 2016. Characterization of silver nanoparticles by green synthesis method using *Pedalium murex* leaf extract and their antibacterial activity. Appl. Nanosci. 6 (3), 399–408.

Auld, D.S., 2001. Zinc Coordination Sphere in Biochemical Zinc Sites, vol. 14. Biomaterials, pp. 271–313.
Barapatre, A., Ramadil, K., Jha, H., 2016. Synergistic antibacterial and antibiofilm activity of silver nanoparticles biosynthesized by lignin-degrading fungus. Biores. Bioprog. 3, 1–13.
Barbara, V., Miao, C., Russell, J.C., Elena, P.I., 2009. Bacterial extracellular polysaccharides involved in biofilm formation. Molecules 14, 2535–2554.
Chan, Y.S., Matdon, M., 2013. Biosynthesis and structural characterization of Ag nanoparticles from white rot fungi. Mater. Sci. Eng. 33, 282–288.
Chulhun, K., Herbert, F.J., 1995. Identification of an essential second metal ion in the reaction mechanism of Escherichia coli adenyloscuccinate synthetase. J. Biol. Chem. 270, 15539–15544.
Christensen, G.D., Christesen, W.A., Simpson, J.J., Younger, L., Baddour, M., Barret, F.F., Melton, D.M., 1985. Adherence of coagulase-negativ *Staphylococci* to plastic tissue culture plates: a quantitative model for adherence of *Staphylococci* to medical devices. J. Clin. Microbiol. 22, 996–1006.
Cotter, J.J., O'Gara, J.P., Mack, D., Casey, E., 2009. Oxygen - mediated regulation of biofilm development is controlled by the alternative sigma factor in *Staphylococcus epidermidis*. Appl. Environ. Microbiol. 75, 261–264.
Fawcett, D., Verduin, J.J., Shah, M., Sharma, S.B., Poinern, G.E.J., 2017. A review of current research into the biogenic synthesis of metal and metal oxide nanoparticles via marine algae and seagrasses. J. Nanosci. 1–15.
Fitzpatrick, F., Humphreys, H., O'Gara, J.P., 2005. The genetics of staphylococcal bio film formation – willa greater understanding of pathogenesis lead to better management of device – related infection? Clin. Microbiol. Infct. 11, 967–973.
Freeman, D.J., Falkiner, F.R., Keane, C.T., 1989. New method for detecting slime production by coagulas negative *Staphylococci*. J. Clin. Pathol. 42, 872–874.
Ganesh, M., Lee, S.G., Jayaprakash, J., Mohankumar, M., Jang, H.T., 2019. *Hydnocarpus alpina* Wt extract mediated green synthesis of ZnO nanoparticle and screening of its anti-microbial, free radical scavenging, and photocatalytic activity. Biocatal.Agri. Biotech. 2019 https://doi.org/10.1016/j.bcab.2019.101129 (in press).
Hood, M.I., Skaar, E.P., 2012. Nutritional immunity : transition metals at the pathogen–host interface. Nat. Publ. Gr 10, 525–537, 2012.
Ishwarya, R., Vaseeharan, B., Kalyani, S., Banumathi, B., Govindarajan, M., Alharbi, N.S., Kadaikunnan, S., Al-Anbr, M.N., Khaled, J.M., Benelli, G., 2018. Facile green synthesis of zinc oxide nanoparticles using *Ulva lactuca* seaweed extract and evaluation of their photocatalytic, antibiofilm and insecticidal activity. J. Photochem. Photobiol., B 178, 249–258.
Ingale, G., Chaudhari, A.N., 2013. Biogenic Synthesis of nanoparticles and potential applications: an eco friendly approach. J. Nanomed.Nanotechol. 4 (2), 165.
Jain, N., Bhargava, A., Majumdar, S., Tarafdar, J.C., Panwar, J., 2011. Extracellular biosynthesis and characterization of silver nanoparticles using *Aspergillus flavus* NJP08: a mechanism perspective. Nanoscale 3, 35–641.
Jayaseelan, C., Rahuman, A.A., Kirthi, A.V., Marimuthu, S., Santhoshkumar, T., Bagavan, A., 2012. Novel Microbial route to synthesize ZnO nanoparticles using *Aeromonas hydrophila* and their activity against pathogenic bacteria and fungi. Spectrochim. Acta 90, 78–84.
Kalishwaralal, K., Deepak, V., Pandian, S.R.K., Kottaisamy, M., Barath Manikanth, S., Kartikeyan, B., Gurunathan, S., 2010. Biosynthesis of silver and gold nanoparticles using *Brevibacterium casei*. Colloids Surf., B 77, 257–262.
Kaviya, S.S.J., Viswanathan, B., 2011. Green synthesis of silver nanoparticles using *Polyalthia longifolia* leaf extract along with D- sorbitol. J. Nanotech. 1–5.
Khalil, K.A., Fouad, H., Elsarnagawy, T., Almajhdi, F.N., 2013. Preparation and characterization of electrospun PGLA/silver composite nanofibres for biomedical applications. Int. J. Elctrochem. Sci. 8, 3483–3493.
Kirthi, A.V., Rahuman, A.A., Rajakumar, G., Marimuthu, S., Santhoshkumar, T., Jayaseelan, C., Elango, G., Abduz Zahir, A., Kamaraj, C., Bagavan, A., 2011. Mater. Lett. 65, 2745–2747.
Korbekandi, H., Iravani, S., 2012. Silver nanoparticles, the delivery of nanoparticles. In: Hashim Abbass A., pp. 5–9.
Kumar, A., Pandey, A.K., Singh, S.S., Shanker, R., Dhawan, A., 2011. Cellular uptake and mutagenic potential of metal oxide nanoparticles in bacterial cells. Chemosphere 83, 1124–1132.
Long, T.C., Saleh, N., Tilton, R.D., Lowry, G.V., Veronesi, B., 2006. Titanium Dioxide (P25) produces reactive oxygen species in immortalized microglia (Bv2): implications for nanoparticle neurotoxicity. Environ. Sci. Technol. 40, 4346–4352.
Magrez, S., Kasas, V., Salicio, N., Pasquier, J., Seo, W., Celio, M., Catsicas, S., Schwaller, B., Forro, L., 2006. Cellular toxicity of carbon-based nanomaterials. Nano Lett. 6, 1121–1125.
Marques, S., Ramos, J.L., 1993. Transcriptional control of the *Pseudomonas putida* TOL plasmid catabolic pathways. Mol. Microbiol. 9, 923–929.
Mytilinaios, I., Bernigaud, I., Belot, V., Lambert, R.J.W., 2014. Microbial growth parameters obtained from the analysis of time to detection data using a novel rearrangement of the Baranyi–Roberts model. J. Appl. Microbiol. 118, 161–174.
Narendhran, S., Sivaraj, R., 2016. Biogenic ZnO nanoparticles synthesized using *L. aculeate* leaf extract and their antifungal activity against plant fungal pathogens. Bull. Mater. Sci. 39, 1–5.
Nel, A., Xia, T., Adler, L.M., Li, N., 2006. Toxic potential of materials at the nano level. Science 311, 622–627.
Prasad, N.V.K.V., Elumalai, E.K., Khatja, S., 2011. Evaluation of the antimicrobial efficacy of phytognic silver nanoparticles. Asian Pac. J. Trop. Biomed. 82–85.
Rauwel, E., Galeckas, A., Rauwel, P., Sunding, M.F., Fjellv, H., 2011. Precursor-dependent blue-green photoluminescence emission of ZnO nanoparticles. J. Phys. Chem. C 115, 25227–25233.
Saravanakumar, A., Ganesh, M., Jayaprakash, J., Jang, H.T., 2015. Biosynthesis of silver nanoparticles using *Cassia tora* leaf extract and its antioxidant and antibacterial activities. J. Ind. Eng. Chem. 28, 277–281.
Sawai, J., Kawada, E., Kanou, F., Igarashi, H., Hashimoto, A., Kokugan, T., Shimizu, M., 1996. Detection of active oxygen generated from ceramic powders having antibacterial activity. J. Chem. Eng. Jpn. 29, 627–633.
Shankar, S.S., Raj, A., Ahmad, A., Sastry, M., 2004. Rapid synthesis of Au, Ag, and bimetallic Au core- Ag shll nanoparticles using neem (*Azadira chtaindica*) leaf broth. J.f Collo. Inter. Sci. 275, 496–502.
Sharma, D., Rajput, J., Kaith, B.S., Kaur, M., Sharma, S., 2010. Synthesis of ZnO nanoparticles and study of their antibacterial and antifungal properties. Thin Solid Films 519 (3), 1224–1229.
Shervani, Z., Yamamoto, Y., 2011. Carbohydrate- directed synthesis of silver and gold nanoparticles: effect of the structure of carbohydrates and reducing agents on the size and morphology of the composites. Carbohydr. Res. 346, 651–658.
Steffy, K., Shanthi, G., Maroky, A.S., Selvakumar, S., 2018. Synthesis and characterization of ZnO phytonanocomposite using Strychnos nux-vomica L. (Loganiaceae) and antimicrobial activity against multidrug-resistant bacterial strains from diabetic foot ulcer. J. Adv. Res. 9, 69–77.
Thaya, R., Malaikozhundan, B., Vijayakumar, S., Sivakamavalli, J., Jeyasekar, R., Shanthi, S., Vaseeharan, B., Ramasamy, P., Sonawane, A., 2016. Chitosan coated Ag/ZnO nanocomposite and their antibiofilm, antifungal and cytotoxic effects on murine macrophages. Microb. Pathog. 100, 124–132.
Wahab, R., Kim, Y.S., Mishra, A., Yun, S.I., Shin, H.S., 2010. Formation of ZnO microflowers prepared via solution process and their antibacterial activity. Nanoscale Res. Lett. 5, 1675–1681.
Wagner, C.D., Naumkin, A.V., Kraut-Vass, A., Allison, J.W., Powell, C.J., Rumble, J.R.J., 2003. NIST X-Ray Photoelectron Spectroscopy Database. National Institute of Standards and Technology, Gaithersburg.
Xiao, L., Liu, C., Chen, X., Yang, Z., 2016. Zinc oxide nanoparticles induced renal toxicity through reactive oxygen species. Food Chem. Toxicol. 90, 76–83.
Xiong, G., Pal, U., Serrano, J.G., Ucer, K.B., Williams, R.T., 2006. Photoluminescence and FTIR study of ZnO nanoparticles: the impurity and defect perspective. Phys. Status Solidi C 3, 577–3581.
Yamamoto, O., 2001. Influence of particle size on the antibacterial activity of zinc oxide. Int. J. Inorg. Mater. 3, 643–646.
Zhang, L., Jiang, Y., Ding, Y., Povey, M., York, D., 2007. Investigation into the antibacterial behaviour of suspensions of ZnO nanoparticles (ZnO nanofluids). J. Nanopart. Res. 9, 479–489.